CORROSION SCIENCE AND TECHNOLOGY, Vol.22, No.1(2023), pp.1~9
[Research Paper]
pISSN 1598-6462 / eISSN 2288-6524
DOI: https://doi.org/10.14773/cst.2023.22.1.1

Inhibitory Effect of Benzoate-intercalated Hydrotalcite with Ce^{3+}-loaded clay on Carbon Steel

Thuy Duong Nguyen[1,†], Thu Thuy Pham[1], Anh Son Nguyen[1], Ke Oanh Vu[1], Gia Vu Pham[1], and To Thi Xuan Hang[1,2,†]

[1]*Institute for Tropical Technology, Vietnam Academy of Science and Technology, 18 Hoang Quoc Viet, Cau Giay, Hanoi, Vietnam*
[2]*Graduate University of Science and Technology, Vietnam Academy of Science and Technology, 18 Hoang Quoc Viet, Cau Giay, Hanoi, Vietnam*

(Received August 04, 2022; Revised September 07, 2022; Accepted October 17, 2022)

This work studied the inhibitory effect of the combination of benzoate-intercalated hydrotalcite (HT-BZ) and Ce^{3+}-loaded clay (Clay-Ce) on carbon steel (CS). HT-BZ was prepared by the co-precipitation method and Clay-Ce was fabricated by a cation exchange reaction. HT-BZ and Clay-Ce were assessed by scanning electron microscopy (SEM) and X-ray diffraction (XRD) coupled with zeta potential measurement. Electrochemical measurements coupled with scanning electron microscopy/energy-dispersive X-ray spectroscopy (SEM/EDX) were used for studying the inhibitory action of the mixture of HT-BZ and Clay-Ce on steel electrodes immersed in 0.1 M NaCl. For comparison, the inhibitory effect of HT-BZ or Clay-Ce alone was also evaluated. The results showed that HT-BZ combined with Clay-Ce provided synergistic inhibition of the CS substrate. The mixture of 0.5 g/L HT-BZ + 0.5 g/L Clay-Ce provided 93.5% inhibition efficiency. The protective mechanism of the HT-BZ + Clay-Ce mixture consisted of the reaction of released BZ and Ce^{3+} and the deposition of HT-BZ and Clay-Ce structures on the CS substrate.

Keywords: *Corrosion inhibition, Carbon steel, Hydrotalcite, Benzoate, Ce^{3+}-loaded clay*

1. Introduction

Organic coatings resistant to aggressive environments were widely used to provide anti-corrosion of steel surfaces [1]. However, organic coatings are prone to water uptake, causing the corrosion of the materials [2]. The inhibitors added in the coatings can limit the water absorption of these coatings and increase the active anti-corrosion for the substrates [3,4]. Among these, hydrotalcite (HTs) and clays have been of great interest due to their ability to act as an inhibitory container for anti-corrosion and their low cost [3,5,6].

Organic/inorganic inhibitor-loaded HT can release inhibitors when exposed to aggressive environments [7,8]. Moreover, invasive ions such as Cl^- were also held by the HT interlayer [7,9]. Yan et al. prepared ZnAlCe HT bearing molybdate (ZnAlCe-MoO_4 HT) and studied their influence on CS corrosion in NaCl solution [10]. The obtained electrochemical measurements indicated that ZnAlCe-MoO_4 HT provided higher protection properties than ZnAl-NO_3 and ZnAl-MoO_4 HT. Additionally, Cl^- can be exchanged with MoO_4^{2-} from ZnAlCe-MoO_4 HT, which decreases of Cl^- concentration in electrolyte solution. The HTs containing organic inhibitors like benzothiazolylthio-succinic acid (BTSA), benzoate (BZ), benzotriazole (BTA), and sebacate (SB) were studied to restrict the corrosion of CS substrates in sodium chloride medium [3,4,6]. The results showed that these organic inhibitors, which were released from the hydrotalcite interlayer, can block the anodic sites on the metal surface. In addition, our previous studies showed that ZnAl-HTs intercalated with BZ at high concentrations had an inhibition efficiency was higher than 90% for CS substrate [3,4].

Due to the rich interstitial chemistry of clay compounds, the efficient replacement of inorganic ions by surfactants or cationic organic molecules can be realized through cation exchange reactions [11,12]. Among layered silicates, clay montmorillonite (MMT) has been most extensively investigated [13]. Organic coatings containing MMT bearing inhibitors showed promise for protection against

†Corresponding author: ntd0801@gmail.com, ttxhang60@gmail.com

metal corrosion [11,12,14,15]. The MMT modified with amino-trimethylphosphonic acid or 8-hydroxyquinoline or indole 3-butyric acid improved protection performance of these epoxy coatings applied on steel substrates [14-16]. Modified MMT enhanced the barrier properties of coatings and played the role of inhibitor container. The Ce^{3+} modified MMT (Ce-MMT) was used in sol-gel films applied on AA2024 surface substrate [11]. The results showed that Ce-MMT significantly enhanced the protection performance of the sol-gel film.

A lot of research has focused on the individual effect of HT or clay but not their combined ability. This motivated us to study inhibition action of HT-BZ combined with clay loading Ce^{3+} on steel substrate. The inhibition action of the mixture of HT-BZ and Clay-Ce was measured using electrochemical measurements coupled with SEM/EDX. For comparison, the inhibition action of individual HT-BZ or Clay-Ce was also studied. The protection action mechanisms of the mixture of HT-BZ and Clay-Ce for steel surface were discussed.

2. Experimental Methods

2.1 Materials

$Zn(NO_3)_2{\cdot}6H_2O$, $Al(NO_3)_3{\cdot}9H_2O$, $Ce(NO_3)_3{\cdot}6H_2O$, and NaOH were obtained from Merck. Sodium benzoate ($C_7H_5O_2Na$) (99%) was obtained from Sigma.

The montmorillonite clay was from Binh Thuan province in Vietnam. This clay had a 2/1 ratio of silica to alumina, and the cation exchange capacity was 100–115 meq/100 g.

2.2 Preparation of HT-BZ

Hydrotalcite bearing benzoate (HT-BZ) was prepared using the co-precipitation reaction [4]. Solution 1 was a salt mixture of $Zn(NO_3)_2$ and $Al(NO_3)_3$ (Zn^{2+}/Al^{3+} molar ratio = 2/1). Solution 2 was an BZ solution with pH adjusted by NaOH solution. Solution 2 was kept under a nitrogen atmosphere at a temperature of 25 ºC and pH = 8 - 9. Solution 1 was added to solution 2 with magnetic stirring. Then the mixture was kept at 50 ºC for 24 h under a nitrogen atmosphere. The precipitation was washed with degassed distilled water and dried at 70 ºC for 48 h.

2.3 Preparation of Clay-Ce

First, 3 g pristine clay was dispersed in 300 mL distilled water containing 3 g $Ce(NO_3)_3{\cdot}6H_2O$. Then, the mixture was stirred at a temperature of 25 ºC for 24 h. The precipitate was washed with distilled water several times. After that, Clay-Ce was dried at 60 ºC in a vacuum oven for 48 h.

2.4 Analytical characterization

Powder X-ray diffraction (XRD) spectra of HT-BZ and Clay-Ce were obtained on Siemens diffractometer D5000 using CuKα radiation (λ = 0.15406 nm) from 1º to 70º in air conditions. The scanning speed was 2.6º/min.

The zeta potential values of the HT-BZ and Clay-Ce were measured on a MALVERN Zetasizer Nano ZS.

Scanning electron microscope (SEM) was used to observe the morphologies of HT-BZ and Clay-Ce. SEM photographs were obtained on Hitachi S-4800.

Steel surfaces after 2 h exposure to NaCl medium without inhibitor and with HT-BZ and Clay-Ce were assessed by SEM/EDX on a JSM-6510LV microscope.

2.5 Electrochemical measurements

Electrochemical tests were done with the three-electrode cell: a platinum auxiliary electrode, a saturated calomel reference electrode (SCE), and a working electrode with an exposed area of 1 cm^2. The electrochemical tests were carried out with a VSP 300 Biologic. The testing solution was a 0.1 M sodium chloride solution. Three concentrations of HT-BZ and Clay-Ce with a total 1 g/L inhibitor concentration were investigated: 1 g/L HT-BZ; 1 g/L Clay-Ce and 0.5 g/L HT-BZ + 0.5 g/L Clay-Ce. The impedance diagrams of all samples were recorded after immersion of 2 h with the frequency range between 100 kHz to 10 mHz, using a sinusoidal voltage of 5 mV. The polarization curves of all samples were performed from -30 mV vs OCP to 300 mV vs OCP (V/SCE) with a sweep speed of 1 mV/s after 2 h immersion. Each measurement was repeated at least three times. Corrosion potential and corrosion current density were determined from polarization curves. The Zfit software supplied by Biologic based on Wagner-Traud equation was used.

3. Results

3.1 Characterization of Clay-Ce and HT-BZ

The presence of Ce^{3+} in clay was identified by XRD

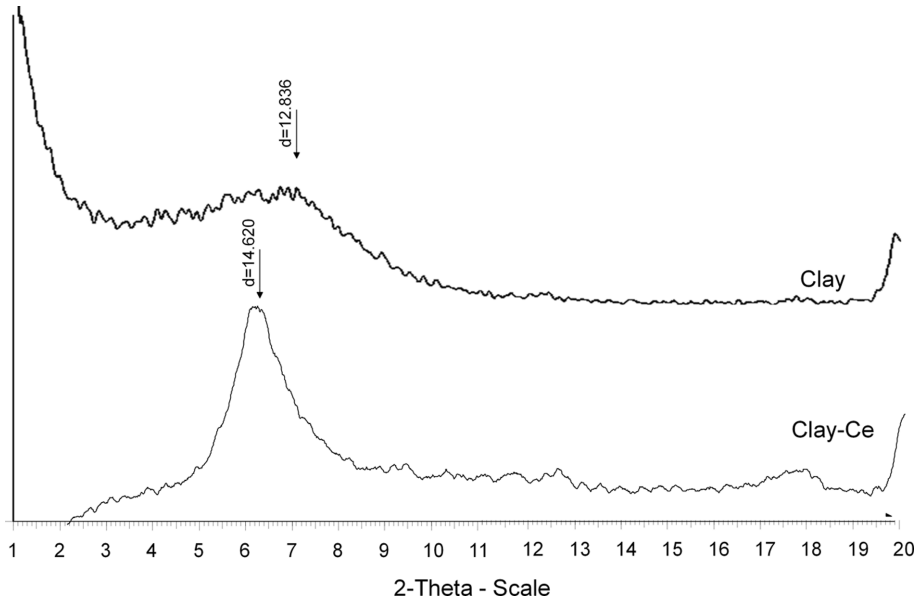

Fig. 1. XRD spectra of clay and Clay-Ce

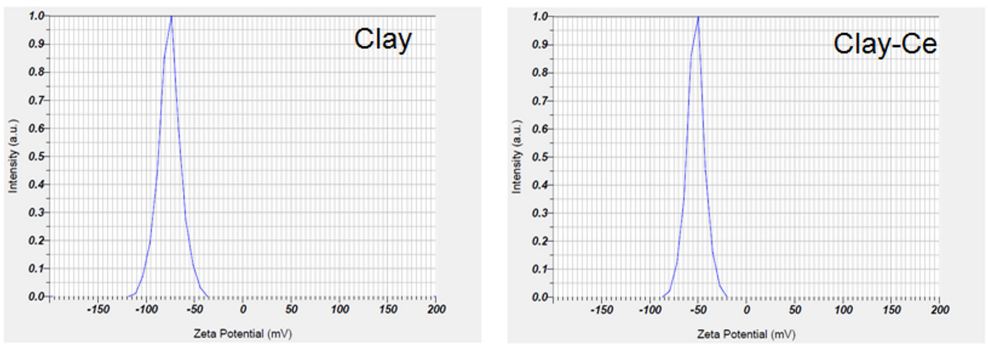

Fig. 2. Zeta potential value of Clay-Ce and pristine clay

analysis. Fig. 1 showed the XRD pattern of pristine clay and Clay-Ce samples. The characteristic peak corresponding to the d(001) plane of the pristine clay appeared at 2θ = 7º for the Clay-Ce sample and 2θ = 6º for original clay sample. Using the Bragg's law, the d-spacing of pristine clay and Clay-Ce was 12.8 Å and 14.6 Å, respectively. The significant increase of d-spacing in the Clay-Ce compared to pristine clay indicated the replacement of Na^+ cations by Ce^{3+} [11].

The surface charge values of the pristine clay and Clay-Ce were determined by zeta potential measurement in water (Fig. 2). The clay concentration was 0.03%. The zeta potentials determined were -76.0 mV and -52.5 mV for pristine clay and Clay-Ce respectively. The negative surface charge of clay was caused by the replacement of some valence of Si(IV) cations in SiO_4 by Al(III). When clay was modified with Ce^{3+}, it was possible that some of the Na^+ in the clay interlayer was replaced by Ce^{3+}, changing the charge of clay-Ce to a more positive value than that of the original clay.

SEM images of pristine clay and Clay-Ce samples (Fig. 3) showed that both pristine clay and Clay-Ce had lamellar structure. The Clay-Ce had the similar particle size as that of the pristine clay but its particles were more separated.

The recorded XRD spectrum and SEM photograph of HT-BZ are shown in Fig. 4. The dominant peaks of HT crystal structure were located at 2θ angles of 5.40º, 11.33º, 22.86º, 34.90º and 60.67º, corresponding to (003), (006), (009), (012) and (110) planes, respectively (Fig. 4a) [4]. The XRD spectrum of HT-BZ presented the (003)

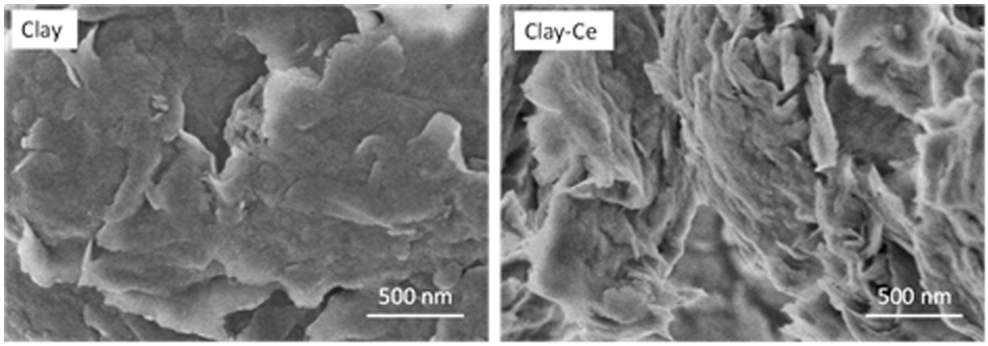

Fig. 3. SEM photographs of Clay-Ce and pristine clay

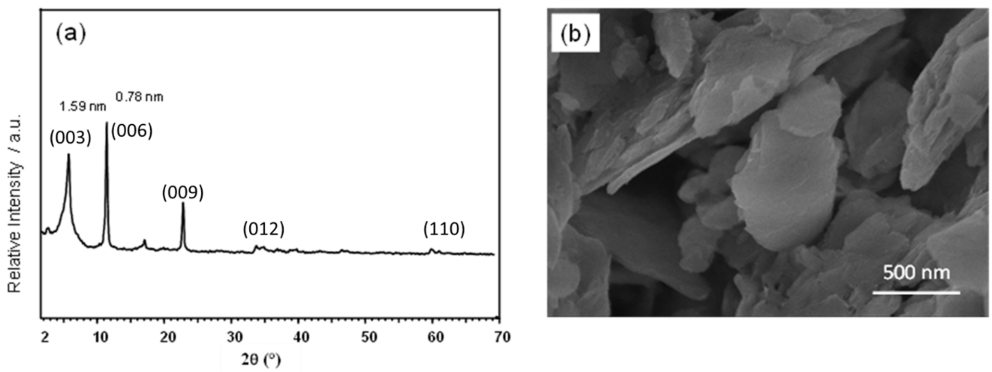

Fig. 4. XRD spectrum (a) and SEM photograph (b) of HT-BZ

reflections corresponding to d-spacing of 1.59 nm and 1.96 nm respectively, which were higher than d-spacing of nitrate hydrotalcite of 0.79 nm [4]. The higher d-spacing of the HT-BZ indicated the accommodation of BZ in the interlayer domain of HT host.

The SEM photographs (Fig. 4b) showed the typical plate-like morphology of HT-BZ with particle sizes about 200 - 500 nm.

3.2 Corrosion inhibition of HT-BZ and Clay-Ce

Inhibition effect of HT-BZ, Clay-Ce and HT-BZ + Clay-Ce mixture for CS was studied with a 1 g/L inhibitor concentration. For a comparison, the corrosion test was also realized for a NaCl solution without any inhibitor. The electrochemical impedance diagrams and polarization curves were measured after 2 h exposure.

Fig. 5 presents the anodic polarization curves measured for steel electrodes immersed in NaCl without inhibitors and with HT-BZ or Clay-Ce or HT-BZ + Clay-Ce mixture. Corrosion potential (E_{corr}), corrosion current density (i_{corr}) and inhibition efficiency are shown in Table 1.

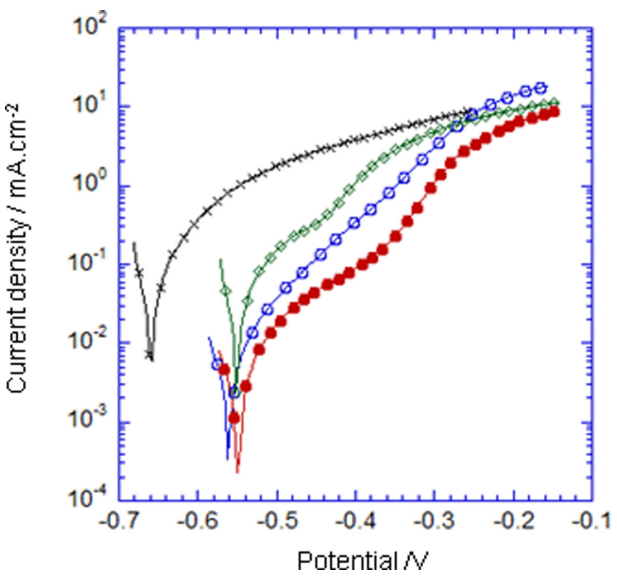

Fig. 5. Anodic polarization curves of steel electrode without inhibitor (x), with 1g/L HT-BZ (o), with 1 g/L Clay-Ce (◊) and with 0.5 g/L HT-BZ+ 0.5 g/L Clay-Ce (●)

The i_{corr} determined for the case without inhibitor was 120 µA.cm^{-2}. The i_{corr} value in the case of HT-BZ or

Clay-Ce was lower compared to the blank sample, at 63.7 μA.cm^{-2} and 87 μA.cm^{-2} respectively. The anodic current density determined for the mixture of HT-BZ and Clay-Ce (23.6 μA.cm^{-2}) was worse than that of HT-BZ or Clay-Ce sample. The lower i_{corr} value of HT-BZ + Clay-Ce mixture in comparison with individual Clay-Ce and HT-BZ can be caused by the simultaneous effects of benzoate released from HT-BZ and Ce^{3+} released from Clay-Ce. Benzoate released from HT-BZ can be adsorbed on CS substrate and impede the anodic corrosion reaction [6]. Moreover, layer structures of hydrotalcite and clay can be deposited on CS substrate. The polarization curves results demonstrated that HT-BZ + Clay-Ce mixture showed anodic inhibitor of CS and combination with Clay-Ce improved the inhibition ability of HT-BZ.

The EIS Nyquist and Bode diagrams of steel electrodes after 2 h immersion in 0.1 M NaCl solution without inhibitor and with HT-BZ and Clay-Ce and HT-BZ + Clay-Ce mixture are presented in Fig. 6. The electric equivalent circuits used for fitting the EIS diagrams are presented in Fig. 7.

Table 1. Corrosion potential and corrosion current density determined from polarization curves

Sample	E_{corr} (mV)	i_{corr} (μA.cm^{-2})
Without inhibitor	-659.0	120.0
1 g/L HT-BZ	-570.0	63.7
1 g/L Clay-Ce	-527.0	87.0
0.5 g/L HT-BZ + 0.5 g/L Clay-Ce	-520.5	23.6

For blank sample and sample with Clay-Ce, the impedance diagrams had only one time constant, which corresponds to electric equivalent circuits of Fig. 7a. For the case with HT-BZ and HT-BZ + Clay-Ce mixture, the EIS diagrams had two time constants, which corresponded to the electric equivalent circuits of Fig. 7b. Inhibition

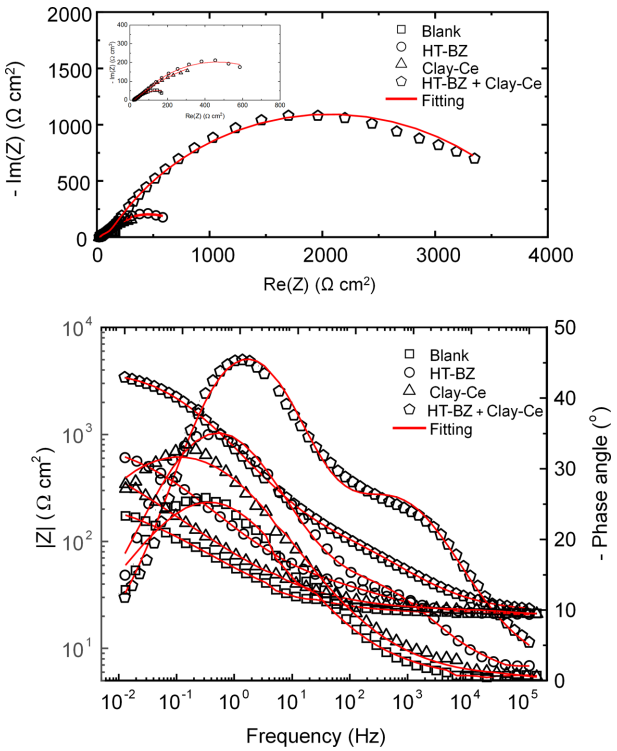

Fig. 6. Impedance diagrams obtained for steel electrode after 2 h exposure in 0.1 M NaCl: without inhibitor (□), with 1 g/L HT-BZ (o), with 1 g/L Clay-Ce (Δ) and with 0.5 g/L HT-BZ+ 0.5 g/L Clay-Ce (⌓)

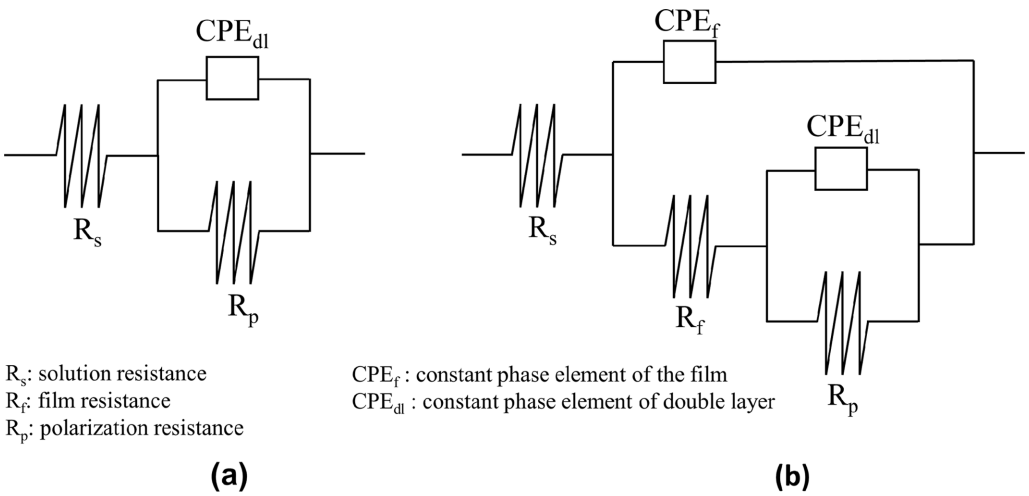

Fig. 7. The electric equivalent circuits used for fitting the EIS diagrams

efficiencies are determined from polarization resistances using equation (1).

$$E\% = (R_p - R_{p0})/R_p \quad (1)$$

Where, R_{p0} is the polarization resistance of sample without inhibitor and R_p is the polarization resistance of sample containing inhibitor. The fitted EIS parameters were shown in Table 2.

The solution resistance of the blank sample was 21 Ω·cm^2. The solution resistance of samples with HT-BZ, Clay-CE and HT-BZ + Clay-Ce mixture were also 21 Ω·cm^2 or 22 Ω·cm^2. This indicated that HT-BZ and Clay-CE at 1 g/L concentrations did not change the resistance of the NaCl medium.

The R_f of sample with HT-BZ was 27 Ω·cm^2, while the R_f of sample with HT-BZ + Clay-Ce mixture was 144 Ω·cm^2. The low R_f for the sample HT-BZ showed a thin and porous film formed on the CS substrate. Higher R_f value obtained for the mixture of HT-BZ and Clay-Ce can be explained by the participation of Clay-Ce in protective film on CS substrate.

The polarization resistance is associated with the corrosion development on the metal surface. Higher R_p value indicates higher corrosion resistance. The R_p of the blank sample was 256 Ω·cm^2. The R_p of sample with HT-BZ, Clay-Ce and HT-BZ + Clay-Ce mixture were higher than that of blank sample and were 1197, 845 and 3919 Ω·cm^2 respectively. The inhibition efficiencies of HT-BZ, Clay-Ce and HT-BZ + Clay-Ce mixture were 78.6%, 69.7% and 93.5% respectively. The EIS results agreed with the polarization curves results. The electrochemical measurement results showed that the mixture of HT-BZ and Clay-Ce presented significantly higher inhibition effect than individual HT-BZ or Clay-Ce.

3.3 Surface analysis

The sample surfaces after 2 h exposure in NaCl solutions without and with inhibitors were also analyzed

Table 2. Fitting EIS parameters of samples

Sample	Rs ($\Omega.cm^2$)	CPE_f ($\Omega^{-1}.s^n.cm^{-2}$)	n_f	R_f ($\Omega.cm^2$)	CPE_{dl} ($\Omega^{-1}.s^n.cm^{-2}$)	n	R_p ($\Omega.cm^2$)	E (%)
Without inhibitor	21				1.12E-02	0.51	256	-
1 g/L HT-BZ	21	7.15E-04	0.58	27	8.39E-03	0.59	1197	78.6
1 g/L Clay-Ce	22				2.80E-03	0.53	845	69.7
0.5 g/L HT-BZ + 0.5 g/L Clay-Ce	22	1.96E-04	0.66	144	2.62E-04	0.72	3919	93.5

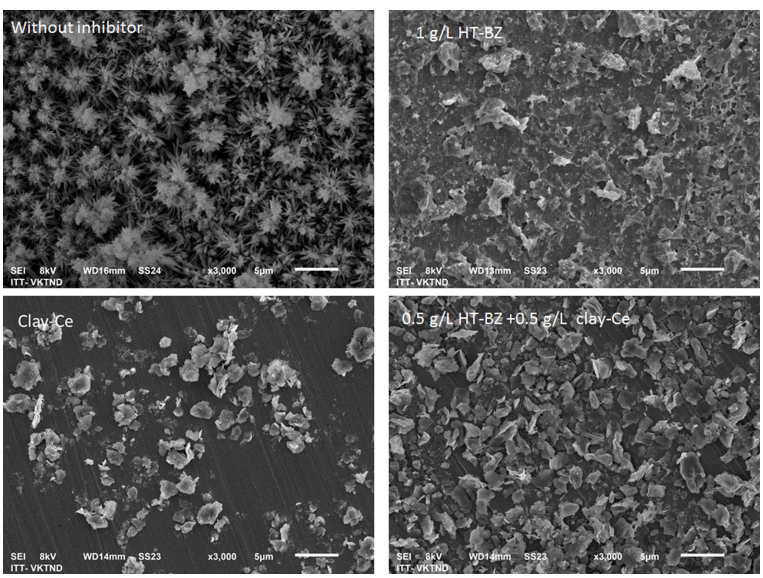

Fig. 8. SEM photographs of samples after 2 h exposure in 0.1 M NaCl

Table 3. Elemental compositions of the steel surfaces after 2 h exposure in 0.1 M NaCl

Sample	Fe (wt%)	O (wt%)	Zn (wt%)	Al (wt%)	Si (wt%)	Ce (wt%)	C (wt%)
Without inhibitor	83.32	8.66	-	-		-	8.02
1 g/L Clay-Ce	75.51	7.35	-	0.36	1.01	11.4	4.36
1 g/L HT-BZ	61.97	11.95	17.03	0.98		-	8.07
0.5 g/L HT-BZ+ 0.5 g/L Clay-Ce	73.40	9.62	6.11	0.60	0.90	4.32	5.05

by SEM/EDX. Fig. 8 presents the SEM photographs of sample surfaces after 2 h exposure. For the blank sample there were structures of iron oxides. For the sample with HT-BZ, the sample surface was almost covered by hydrotalcite structures. For the sample with Clay-Ce, there were clay structures, but the sample surface was not covered totally by clay structures. For the sample with the mixture of HT-BZ and Clay-Ce, hydrotalcite and clay layers covered almost the sample surface. These surface analysis results explained the high inhibition effect obtained with the HT-BZ + Clay-Ce mixture.

The surface elemental compositions after 2 h exposure of the blank sample and samples with HT-BZ and Clay-Ce and HT-BZ + Clay-Ce mixture were determined by EDX. The elemental analysis results of the surface are shown in Table 3.

After 2 h exposure, for the blank sample, iron and oxygen are detected. The Fe content and O contents were 83.32% and 8.66% respectively. For the sample with HT-BZ, the Al and Zn were detected, and the Al and Zn content were 0.98% and 17.03% respectively. This indicated ZnAl hydrotalcite deposited on the sample surface. For samples with Clay-Ce, the Al, Si and Ce were observed with contents of 0.36%, 1.01% and 11.4% respectively. These results demonstrated the clay structure and Ce on the sample surface. For the mixture of HT-BZ and Clay-Ce we observed all elements present for the mixtures with HT-BZ and Clay-Ce individually. These results confirmed the deposition of hydrotalcite and clay structures on the CS surface.

3.4 Discussion

The action mechanism of HT-BZ + Clay-Ce mixture on CS substrate during exposure to 0.1 M NaCl was presented in Fig. 9. During exposure to 0.1 M NaCl, Fe^{2+} and Fe^{3+} cations were formed on surface substrate due to anodic reactions (Eq. 2 and 3), while hydroxyl anions were formed due to oxygen reduction (Eq. 4) (Fig. 9a)

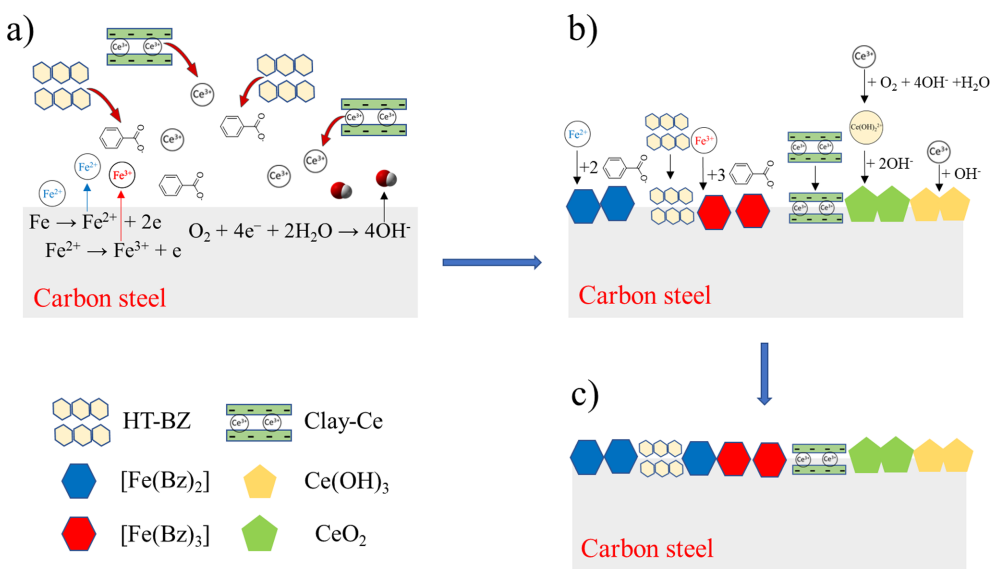

Fig. 9. Protection action mechanism of HT-BZ + Clay-Ce mixture on steel substrate

[5]. The released Ce^{3+} cations from Clay-Ce could react with the OH- anions to form $Ce(OH)_3$ and CeO_2 at the cathodic areas (Eq. 5-7) (Fig. 9b) [17]. These species helped to seal at the cathodic areas, thus the pitting growth can stop and the corrosion process at these areas can be slowed [17]. At the anodic areas, the Fe^{2+} and Fe^{3+} cations reacted with the released BZ anions from the HT-BZ forming the mixture of $[Fe(Bz)_2]$ and $[Fe(Bz)_3]$ complexes (Eq. 8 and 9), which prevented the metal dissolution (Fig. 9b) [3]. Moreover, the deposition of HT-BZ and Clay-Ce on the CS surface formed a protective barrier layer, which can delay the corrosion development (Fig. 9c) [3].

$$Fe \rightarrow Fe^{2+} + 2e \quad (2)$$

$$Fe^{2+} \rightarrow Fe^{3+} + e \quad (3)$$

$$O_2 + 4e + 2H_2O \rightarrow 4OH^- \quad (4)$$

$$Ce^{3+} + 3OH^- \rightarrow Ce(OH)_3 \quad (5)$$

$$4Ce^{3+} + O_2 + 4OH^- + 2H_2O \rightarrow 4Ce(OH)_2^{2+} \quad (6)$$

$$Ce(OH)_2^{2+} + 2OH^- \rightarrow CeO_2 + 2H_2O \quad (7)$$

$$Fe^{2+} + 2Bz^- \rightarrow [Fe(Bz)_2] \quad (8)$$

$$Fe^{3+} + 3Bz^- \rightarrow [Fe(Bz)_3] \quad (9)$$

4. Conclusions

The combination of hydrotalcite bearing benzoate (HT-BZ) and clay loading Ce^{3+} (Clay-Ce) was investigated for corrosion inhibition of carbon steel in 0.1 M NaCl solution. The results indicated that a mixture of HT-BZ and Clay-Ce provided a synergistic inhibition effect for carbon steel. The corrosion inhibition efficiency of the 0.5 g/L HT-BZ + 0.5 g/L Clay-Ce mixture was 93.5%. The corrosion inhibition efficiency of HT-BZ and Clay-Ce individually with 1 g/L concentrations were only 78.6% and 69.7% respectively. Corrosion protection mechanism of the HT-BZ + Clay-Ce mixture consisted of the reaction of released BZ and Ce^{3+} and the deposition of HT-BZ and Clay-Ce on the steel substrate.

Acknowledgments

The authors gratefully acknowledge the financial support of the Vietnam Academy of Science and Technology under the project number NCVCC 13.05/21-21 for senior researchers and the project number TDVLTT.04/21-23.

References

1. M. Tabish, J. Zhao, J. Wang, M.J. Anjum, Y. Qiang, Q. Yang, M.A. Mushtaq, G. Yasin, Improving the corrosion protection ability of epoxy coating using CaAl LDH intercalated with 2-mercaptobenzothiazole as a pigment on steel substrate, *Progress in Organic Coatings*, **165**, 106765 (2022). Doi: https://doi.org/10.1016/j.porgcoat.2022.106765
2. L. Garden, R.A. Pethrick, A dielectric study of water uptake in epoxy resin systems, *Journal of Applied Polymer Science*, **134**, 44717 (2017). Doi: https://doi.org/10.1002/app.44717
3. D. T. Nguyen, H. T. X. To, J. Gervasi, Y. Paint, M. Gonon, M.-G. Olivier, Corrosion inhibition of carbon steel by hydrotalcites modified with different organic carboxylic acids for organic coatings, *Progress in Organic Coatings*, **124**, 256 (2018). Doi: https://doi.org/10.1016/j.porgcoat.2017.12.006
4. D. Nguyen Thuy, H. To Thi Xuan, A. Nicolay, Y. Paint, M.-G. Olivier, Corrosion protection of carbon steel by solvent free epoxy coating containing hydrotalcites intercalated with different organic corrosion inhibitors, *Progress in Organic Coatings*, **101**, 331 (2016). Doi: https://doi.org/10.1016/j.porgcoat.2016.08.021
5. D. Dwivedi, K. Lepková, T. Becker, Carbon steel corrosion: a review of key surface properties and characterization methods, *RSC Advances*, **7**, 4580 (2017). Doi: https://doi.org/10.1039/C6RA25094G
6. B. Wu, J. Zuo, B. Dong, F. Xing, C. Luo, Study on the affinity sequence between inhibitor ions and chloride ions in Mg Al layer double hydroxides and their effects on corrosion protection for carbon steel, *Applied Clay Science*, **180**, 105181 (2019). Doi: https://doi.org/10.1016/j.clay.2019.105181
7. J. Rodriguez, E. Bollen, T. D. Nguyen, A. Portier, Y. Paint, M. G. Olivier, Incorporation of layered double hydroxides modified with benzotriazole into an epoxy resin for the corrosion protection of Zn-Mg coated steel,

Progress in Organic Coatings, **149**, 105894 (2020). Doi: https://doi.org/10.1016/j.porgcoat.2020.105894

8. T. D. Nguyen, A. S. Nguyen, B. A. Tran, K.O. Vu, D. L. Tran, T. T. Phan, N. Scharnagl, M. L. Zheludkevich, T. X. H. To, Molybdate intercalated hydrotalcite/graphene oxide composite as corrosion inhibitor for carbon steel, *Surface and Coatings Technology*, **399**, 126165 (2020). Doi: https://doi.org/10.1016/j.surfcoat.2020.126165
9. G. J. Ayemi, S. Marcelin, S. Thérias, F. Leroux, B. Normand, Synergy effect between layer double hydroxide (LDH) and EDDS for corrosion inhibition of carbon steel, *Applied Clay Science*, **222**, 106497 (2022). Doi: https://doi.org/10.1016/j.clay.2022.106497
10. H. Yan, J. Wang, Y. Zhang, W. Hu, Preparation and inhibition properties of molybdate intercalated ZnAlCe layered double hydroxide, *Journal of Alloys and Compounds*, **678**, 171 (2016). Doi: https://doi.org/10.1016/j.jallcom.2016.03.281
11. T. T. Thai, A. T. Trinh, M.-G. Olivier, Hybrid sol–gel coatings doped with cerium nanocontainers for active corrosion protection of AA2024, *Progress in Organic Coatings*, **138**, 105428 (2020). Doi: https://doi.org/10.1016/j.porgcoat.2019.105428
12. S. Akbarzadeh, L. Sopchenski Santos, V. Vitry, Y. Paint, M.-G. Olivier, Improvement of the corrosion performance of AA2024 alloy by a duplex PEO/clay modified sol-gel nanocomposite coating, *Surface and Coatings Technology*, **434**, 128168 (2022). Doi: https://doi.org/10.1016/j.surfcoat.2022.128168
13. S. Sinha Ray, M. Okamoto, Polymer/layered silicate nanocomposites: a review from preparation to processing, *Progress in Polymer Science*, **28**, 1539 (2003). Doi: https://doi.org/10.1016/j.progpolymsci.2003.08.002
14. T. T. X. Hang, T. A. Truc, M.-G. Olivier, C. Vandermiers, N. Guérit, N. Pébère, Corrosion protection mechanisms of carbon steel by an epoxy resin containing indole-3 butyric acid modified clay, *Progress in Organic Coatings*, **69**, 410 (2010). Doi: https://doi.org/10.1016/j.porgcoat.2010.08.004
15. T. A. Truc, T. T. Thuy, V. K. Oanh, T. T. X. Hang, A. S. Nguyen, N. Caussé, N. Pébère, 8-hydroxyquinoline-modified clay incorporated in an epoxy coating for the corrosion protection of carbon steel, *Surfaces and Interfaces*, **14**, 26 (2019). Doi: https://doi.org/10.1016/j.surfin.2018.10.007
16. T. Trinh Anh, H. To Thi Xuan, O. Vu Ke, E. Dantras, C. Lacabanne, D. Oquab, N. Pébère, Incorporation of an indole-3 butyric acid modified clay in epoxy resin for corrosion protection of carbon steel, *Surface and Coatings Technology*, **202**, 4945 (2008). Doi: https://doi.org/10.1016/j.surfcoat.2008.04.092
17. Y. Morozov, L. M. Calado, R. A. Shakoor, R. Raj, R. Kahraman, M. G. Taryba, M. F. Montemor, Epoxy coatings modified with a new cerium phosphate inhibitor for smart corrosion protection of steel, *Corrosion Science*, **159**, 108128 (2019). Doi: https://doi.org/10.1016/j.corsci.2019.108128